Journal of Biomechanics 88 (2019) 138–147

Contents lists available at ScienceDirect

Journal of Biomechanics

journal homepage: www.elsevier.com/locate/jbiomech
www.JBiomech.com

Numerical simulations of bone remodelling and formation following nucleotomy

Andrea Calvo-Echenique [a], Maxim Bashkuev [b], Sandra Reitmaier [b], Amaya Pérez-del Palomar [a], Hendrik Schmidt [b,*]

[a] Group of Biomaterials. Mechanical Engineering Department, Aragón Institute of Engineering Research (I3A), University of Zaragoza, Zaragoza, Spain
[b] Julius Wolff Institut, Charité – Universitätsmedizin Berlin, Berlin, Germany

ARTICLE INFO

Article history:
Accepted 22 March 2019

Keywords:
Lumbar spinal fusion surgery
Bone healing
Bone remodelling
Nucleotomy
Internal fixation

ABSTRACT

Nucleotomy is the gold standard treatment for disc herniation and has proven ability to restore stability by creating a bony bridge without any additional fixation. However, the evolution of mineral density in the extant and new bone after nucleotomy and fixation techniques has to date not been investigated in detail. The main goal of this study is to determine possible mechanisms that may trigger the bone remodelling and formation processes.

With that purpose, a finite element model of the L4–L5 spinal segment was used. Bone mineral density (BMD), new tissue composition, and endplate deflection were determined as indicators of lumbar fusion. A bone-remodelling algorithm and a tissue-healing algorithm, both mechanically driven, were implemented to predict vertebral bone alterations and fusion patterns after nucleotomy, internal fixation, and anterior plate placement.

When considering an intact disc height, neither nucleotomy nor internal fixation were able to provide the necessary stability to promote bony fusion. However, when 75% of the disc height was considered, bone fusion was predicted for both techniques. By contrast, an anterior plate allowed bone fusion at all disc heights. A 50% disc-height reduction led to osteophyte formation in all cases. Changes in the intervertebral disc tissue caused BMD alterations in the endplates.

From this observations it can be drawn that fusion may be self-induced by controlling the mechanical stabilisation without the need of additional fixation. The amount of tissue to be removed to achieve this stabilisation remains to be determined.

1. Introduction

Nucleotomy with its long and distinguished history is considered the gold standard for the surgical treatment of disc herniation (Maroon, 2002; Postacchini and Postacchini, 2011). Although widely debated, there remains no consensus regarding the amount of nucleus pulposus (NP) tissue to be removed during surgery to achieve the ideal compromise between the beneficial relief of painful nerve-root impingement, and potential adverse effects including segmental instability, which boost the degenerative cascade and thus pain recurrence (Ivicsics et al., 2014).

To avoid the progression of disc degeneration following nucleotomy, dynamic stabilisation systems were demonstrated to be promising tools (Putzier et al., 2005). However, different animal-model studies have shown a recovery of segmental stability without applying additional stabilising instrumentation (Crisco et al., 1990; Toth et al., 2017). Rather, controlled instability (by allowing antero-posterior segmental translations of 2 mm) was found to enhance bone formation in sheep (Foster et al., 2002). Additionally, in humans, facetectomy is a part of the non-instrumented posterolateral fusion approaches with equal postoperative patient satisfaction compared to instrumented surgeries (Pourtaheri et al., 2015), and can result in stabilisation in patients with proven degenerative spondylolisthesis (Pateder and Benzel, 2010). Exploiting the natural reparative capacities of the body would avoid implant-related complications, with significant reductions among others of surgical time and blood loss (Nasser et al., 2010; Thompson et al., 1990).

Recent ovine studies demonstrated a stiffening effect of spinal segments six months postoperatively after destabilising interventions like facetectomy and nucleotomy (Reitmaier et al., 2017).

* Corresponding author at: Julius Wolff Institut Charité – Universitätsmedizin Berlin, CVK, Institutsgebäude Süd/Südstraße 2, Augustenburger Platz 1, 13353 Berlin, Germany.
E-mail address: hendrik.schmidt@charite.de (H. Schmidt).

https://doi.org/10.1016/j.jbiomech.2019.03.034
0021-9290/

With regard to nucleotomy, the authors proposed various hypotheses for the initiation of a remodelling cascade: (i) osteoblastic progenitor-cell invasion because of the opening of the subchondral vascular network as a consequence of endplate (EP) damage, (ii) the osteogenic transformation of residing cells within the NP because of degeneration by increased osteoprotegerin levels, immunopositivity for Runx2 and the presence of alkaline-phosphatase activity and/or (iii) a progressive ossification of the peridiscal ligaments because of increased segmental motion with subsequent inflammation, fibrosis, and calcification by significant up-regulation of angiopoietin-like protein 2 and transforming growth factor-β (Nakamura et al., 2014; Wang et al., 2015).

The EP between the vertebral body and the intervertebral disc is an important structure for disc nutrition (Holm, 1993; Urban, 1993), and is known to deform significantly under compressive loads (Brinckmann et al., 1983). Mechanically, it appears reasonable that abnormal deformation patterns following nucleotomy (Frei et al., 2001) may induce remodelling processes in the EP and underlying trabecular bone, which compromise the nutrition of a healthy intervertebral disc. Given a (slightly) degenerated disc, however, the altered mechanical environment after nucleotomy might trigger the ossification of the intervertebral space.

The purpose of this numerical analysis therefore was to assess the pro- and anti- osteogenic mechanical consequences of nucleotomy for the intervertebral space. We hypothesized that with time, a more extensive EP deformation together with a higher bone mineral density of the EP region, and a decreased disc height will constitute promoting factors for the ossification of the intervertebral space after nucleotomy. These investigations could help us to better understand why in a proportion of patients the segment stiffened with time after surgical destabilization even without the use of implants.

2. Material and methods

2.1. Finite element (FE) model

A FE model of an intact human L4–L5 FSU was developed. The geometrical parameters were taken from Panjabi et al. (1993, 1992). The model consists of cancellous and cortical bones, posterior bony elements, annulus fibrosus (AF), NP, cartilaginous and bony EPs and seven ligaments. Additionally, an anterior plate (AP) and an internal fixator (IF) were modelled to simulate two different stabilisation scenarios following nucleotomy.

Except for the collagen fibres and ligaments, first-order hexahedral elements were used for the intact model. The fibres, organised in concentric layers, and the ligaments (anterior and posterior longitudinal ligaments, intertransverse, interspinous and supraspinous ligaments, capsular ligament and ligamentum flavum) were represented by membrane elements with nonlinear properties (Schmidt et al., 2007, 2006). Twelve criss-cross fibre layers were considered in the radial direction. The fibre angles to the disc mid-height plane varied from ±45° at the innermost layer to ±30° at the outer periphery (Holzapfel et al., 2005). The articulating facet surfaces were modelled using frictionless surface-to-surface contacts. In the present study, the initial gap between the articulating surfaces was set at 0.2 mm. The AP was modelled using 6 mm-thick shell elements, while the posterior screws and rods were meshed with 5-mm-diameter beam elements.

The annulus ground substance and the NP were modelled using the Mooney-Rivlin hyperelastic material model (Schmidt et al., 2007, 2006). The stress-strain behaviour of the annular fibres and ligaments were described by non-linear curves taken from previous elastostatic studies (Schmidt et al., 2007, 2006). The material properties are summarised in Table 1.

2.2. Bone-remodelling algorithm

An adaptive bone-remodelling algorithm (Huiskes et al., 1987) was implemented to regulate the bone mineral density (BMD) ρ of the vertebrae according to the strain energy density (SED) (Carter et al., 1987; Mullender and Huiskes, 1995). A cubic relationship between BMD and Young's modulus E was employed according to Carter and Hayes (1977):

$$E = 3790\rho^3 \tag{1}$$

The SED divided by the cube of the BMD was used as the mechanical stimulus to avoid diverging solutions typical for stress-driven models. A piecewise-linear relationship between the stimulus and the rate of BMD change (Fig. 1b) was assumed:

$$\frac{dBMD}{dt} = \begin{cases} R(1+s+h), & S^i \geq (1+s+h)S^{ref} \\ R\left(S^i/S^{ref} - (1+s)\right), & (1+s+h)S^{ref} > S^i > (1+s)S^{ref} \\ 0, & (1+s)S^{ref} \geq S^i \geq (1-s)S^{ref} \\ R\left(S^i/S^{ref} - (1-s)\right), & (1-s)S^{ref} > S^i > (1-s-h)S^{ref} \\ R(1-s-h), & S^i \leq (1-s-h)S^{ref} \end{cases} \tag{2}$$

where R is the slope of the remodelling rate, h is the width of the positive slope zones and $2s$ the width of the "lazy zone", in which bone structure remains unchanged and the rate of BMD change is likely limited by mechanical strength (Beaupré et al., 1990; Carter, 1984). Here, R was set to 0.1 and the value of both h and s was set to 0.15. The reference stimulus was computed as the mean of the stimulus in the intact model. The simulations with the intact model started with a uniform BMD of 0.4 g/cm^3 and run until an equilibrium density distribution was attained. Upper and lower limits of 1.6 g/cm^3 and 0.1 g/cm^3, respectively, were defined, beyond which no change in BMD was allowed.

Table 1
Material properties used for the different spinal structures, newly formed tissues and implants.

Materials	E (MPa)		ν
Cortical bone[1]	10,000		0.325
Cancellous bone[1]	100		0.325
Posterior elements[1]	3500		0.325
Cartilaginous endplates[2]	23		0.4
Facet cartilage[3]	35		0.4
Titanium[4]	100,000		0.33
	C_1	C_2	ν
Nucleus pulposus[5]	0.12	0.09	0.499
Annular matrix[6]	0.56	0.14	0.45
Annular fibres[7]	non-linear stress-strain curves		
Ligaments[8]	non-linear stress-strain curves		
Tissue healing	E (MPa)		ν
Granular tissue[9]	0.2		0.167
Fibrous tissue[9]	2		0.167
Cartilage[9]	10		0.167
New bone[9]	1000		0.325

C_1 and C_2: material parameters used for the Mooney–Rivlin formulation. E: Young's modulus, ν: Poisson's ratio.
Values were taken from:
[1] Argoubi and Shirazi-Adl (1996).
[2] Lu et al. (1996).
[3] Schmidt et al. (2012).
[4] Wood and Favor (1972).
[5] Smit (1996).
[6] Goel et al. (1995).
[7] Shirazi-Adl et al. (1986).
[8] Chazal et al. (1985) and Pintar et al. (1992).
[9] Lacroix and Prendergast (2002).

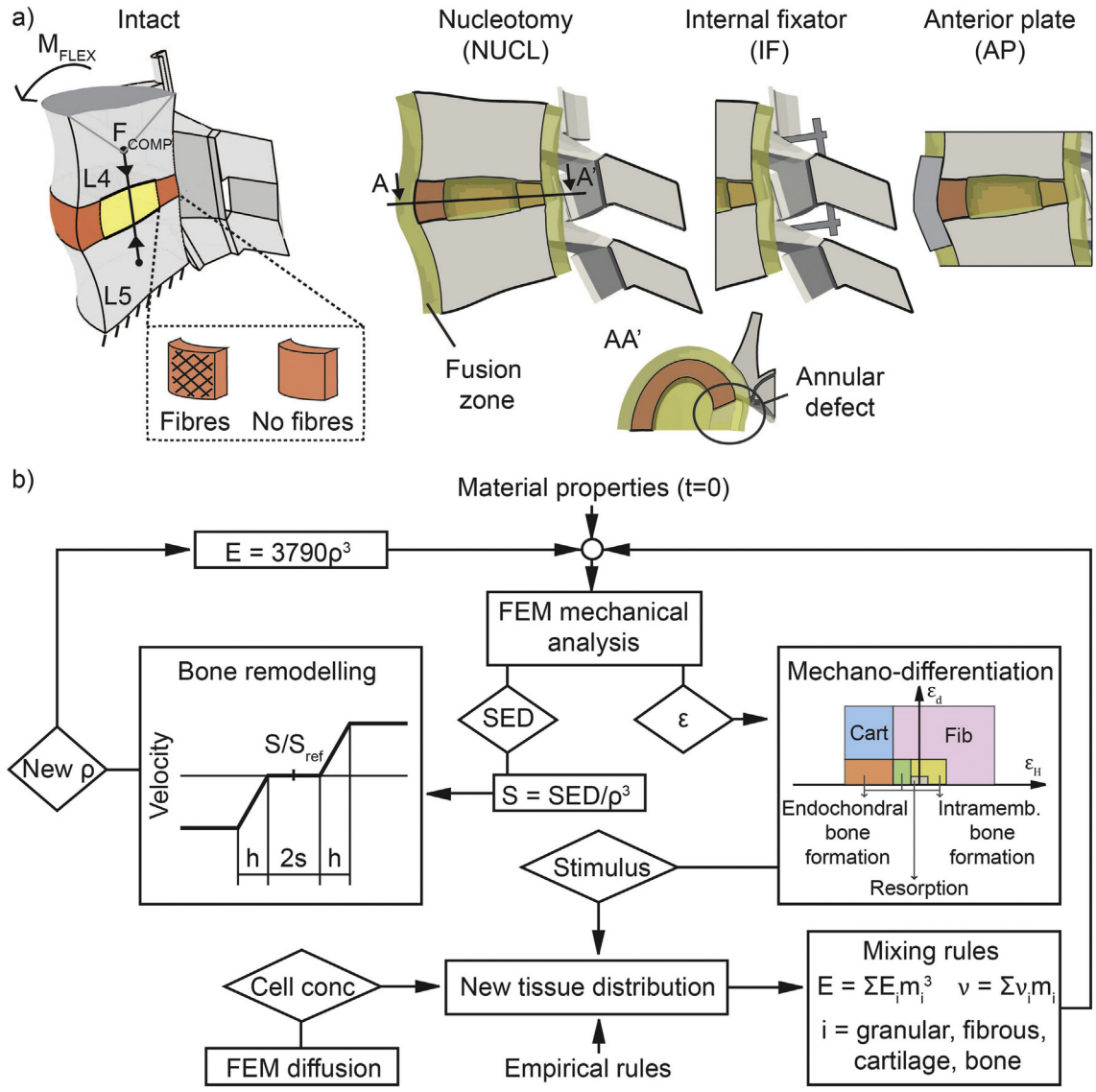

Fig. 1. Finite element model (FEM) of the intact, nucleotomised and instrumented functional spinal unit (a). The fusion zone defines the region where new tissue can be formed. (b) Flow chart of the bone-remodelling and tissue-healing processes. The remodelling process and the mechano-differentiation algorithm are based on the studies of Huiskes et al. (1987) and Claes and Heigele (1999), respectively. ε_d and ε_H distortional and hydrostatic strain, respectively; E Young's modulus; ν Poisson's ratio; m: tissue fraction; SED strain energy density; BMD bone mineral density; h and s parameters defining the bone remodelling algorithm.

2.3. Tissue-healing algorithm

In the nucleotomised models, the space left by the removed tissue (nucleus, cartilage EPs and annular defect) as well as a 5-mm-thick area around the segment were assumed eligible for new tissue formation. Except for the remaining annulus tissue, fully vascularised granulation tissue was assumed to initially occupy these regions. Precursor cell migration from the bone marrow into the granulation tissue was modelled as a diffusive process, with

$$dn/dt = D\nabla^2 n \tag{3}$$

where the cell density n is determined from the diffusion coefficient D, which was specifically chosen as $D = 0.8$ mm^2/iteration for the granulation tissue and as $D = 0.2$ mm^2/iteration for the remaining AF (Kelly and Prendergast, 2005). The cell origin was modelled as a constant concentration at the centre of the vertebral EPs, whereas the maximal cell density was normalised to 1.

In each iteration, the mechanical stimuli (distortional equivalent strain ε_d and hydrostatic strainε_H, Eqs. (4) and (5) were calculated according to the adapted mechano-regulation theory proposed by Claes and Heigele (1999):

$$\varepsilon_d = \frac{2}{3}\sqrt{\left[(\varepsilon_1-\varepsilon_2)^2+(\varepsilon_2-\varepsilon_3)^2+(\varepsilon_1-\varepsilon_3)^2\right]} \tag{4}$$

$$\varepsilon_H = \frac{1}{3}\mathrm{tr}(\underline{\epsilon}) \tag{5}$$

where ε_1, ε_2 and ε_3 are principal strains and $\underline{\epsilon}$ is the strain tensor.

Whether the cell differentiation, tissue destruction, intramembranous or endochondral ossification, bone resorption or development of fibrous tissue into cartilage took place was determined based on the local stimuli values along with a set of additional conditions (Table 2) similar to those considered by Shefelbine et al. (2005). During differentiation, the available precursor cells in each element were allowed to differentiate into fibroblasts, chondrocytes, or osteoblasts and produce their respective tissue phenotypes (Fig. 1b). The differentiation rates are 0.1, 0.1, and 0.2 per iteration for the precursor cells, chondroblasts, and fibroblasts,

Table 2
Summary of empirical rules employed in the tissue healing algorithm.

Event	Stimuli	Additional rules
Tissue destruction[1]	$\varepsilon_H > 5\%$ OR $\varepsilon_d > 15\%$	
Fibrous tissue formation	$(-1\% < \varepsilon_H < 5\%$ AND $5\% < \varepsilon_d < 15\%)$ OR $(1\% < \varepsilon_H < 5\%$ AND $\varepsilon_d < 15\%)$	
Cartilage tissue formation	$-5\% < \varepsilon_H < -1\%$ AND $5\% < \varepsilon_d < 15\%$	(Cartilage fraction < 25% AND bone fraction < 75%)[1] OR (Cartilage fraction > 25% AND (granular fraction > 0 OR fibrous fraction > 0))[1]
Endochondral ossification	$-5\% < \varepsilon_H < -0.1\%$ AND $\varepsilon_d < 5\%$	Tissue vascularized AND Bone fraction in neighbouring elements > 25%[3] AND Cartilage fraction > 25%[1]
Intramembranous ossification	$(-0.1\% < \varepsilon_H < 1\%$ AND $1\% < \varepsilon_d < 5\%)$ OR $(0.1\% < \varepsilon_H < 1\%$ AND $\varepsilon_d < 1\%)$	Tissue vascularized AND Bone fraction in neighbouring elements > 25%[3] AND Cartilage fraction < 25%[1]
Tissue resorption[2]	$-0.1\% < \varepsilon_H < 0.1\%$ AND $\varepsilon_d < 1\%$	

[1] Adopted from Shefelbine et al. (2005).
[2] Adopted from Postigo et al. (2014).
[3] Bone formation was only allowed to occurs on the surfaces of extant bone (Claes and Heigele, 1999; Uhthoff and Rahn, 1981).

respectively, while the resorption rate was 0.05/iteration, adjusted from (Isaksson et al., 2008) to avoid instabilities.

After evaluating the differentiation rules, the new material properties were calculated for each element based on the updated tissue composition as follows:

$$E = E_{gran}m_{gran}^3 + E_{fib}m_{fib}^3 + E_{cart}m_{cart}^3 + E_{bone}m_{bone}^3 \quad (6)$$

$$\nu = \nu_{gran}m_{gran} + \nu_{fib}m_{fib} + \nu_{cart}m_{cart} + \nu_{bone}m_{bone} \quad (7)$$

with $m_{gran} + m_{fib} + m_{cart} + m_{bone} = 1$.

where E is the Young's modulus and ν – the Poisson's ratio, m_{gran}, m_{fib}, m_{cart}, and m_{bone} are the volumetric fractions of granular tissue, fibrous tissue, cartilage, and bone, respectively. The cubic and linear relationships were chosen following Carter and Hayes (1977) and Shefelbine et al. (2005), respectively.

During the tissue healing simulations, the bone remodelling process within the vertebral bodies continued starting from the equilibrium bone density distribution of the intact model.

2.4. Boundary and loading conditions

An iterative procedure (Fig. 1b) was implemented to model bone-remodelling and tissue-healing processes in a lumbar FSU. The load was applied in two steps: first axial compression of 500 N was applied as a follower load; then, a flexion moment of 7.5 N m was added in the following step. The stimulus was calculated as the weighted mean of the results considering 75% of pure compression and 25% compression plus flexion. This assumption is in agreement with Rohlmann et al. (2014), who found that humans spend 20–25% of the entire day with the lumbar spine flexed. To investigate the role of annular fibres, the bone-remodelling simulation of the intact segment was run with and without fibres. Once the BMD reached equilibrium, the entire NP and cartilaginous EP were removed, a 1-cm-wide defect was created in the posterior portion of the AF and an external region for possible osteophyte formation was added. Consequently, the disc height (DH) was reduced to 75 and 50% of the initial height to mimic the DH loss caused by material removal. In additional simulations, the models were supplied with either an AP or IF to study the effects of these devices in the healing process. The described algorithms were implemented in PYTHON 2.7 and the simulations were run in ABAQUS 6.14 (SIMULIA, Providence, RI, USA).

3. Results

3.1. Bone remodelling of the intact segment

The remodelling process started with a uniform increase in the BMD in the entire vertebral body. Progressively, dense cortical shells and EPs formed around a softer inner core (Fig. 2). In the final stages, bone resorption occurred in the anterior and posterior portions of the cancellous bone close to the EP of the adjacent segments. Following 100 iterations, the equilibrium had been attained in the intact models with and without fibres. Although in some areas of the cortical shell and the EPs the stimulus remained high (Fig. 2a), the maximum BMD had already been achieved in these regions and no further density change was possible (Fig. 2b). Removal of the fibres shifted the load sharing in the disc towards the annulus from 43.8% to 49.6%. Accordingly, the BMD decreased in the middle region and increased in the periphery, except in the posterior part of the top vertebra, where a decrease was seen (Fig. 2c). However, the variation of the median values was <3% in the intact model and the difference was even lower after nucleotomy. Because the fibres displayed only a minor influence in the intact and nucleotomy models, in the following, only results from the models with fibres are presented.

3.2. Tissue healing after nucleotomy with and without stabilisation

New bone formation, as well as BMD distributions in the vertebrae, displayed different patterns for each investigated case (Fig. 3). When retaining the initial DH (100%) in the nucleotomy without instrumentation and with IF, both models failed to converge after 15 iterations because of excessive distortion of the

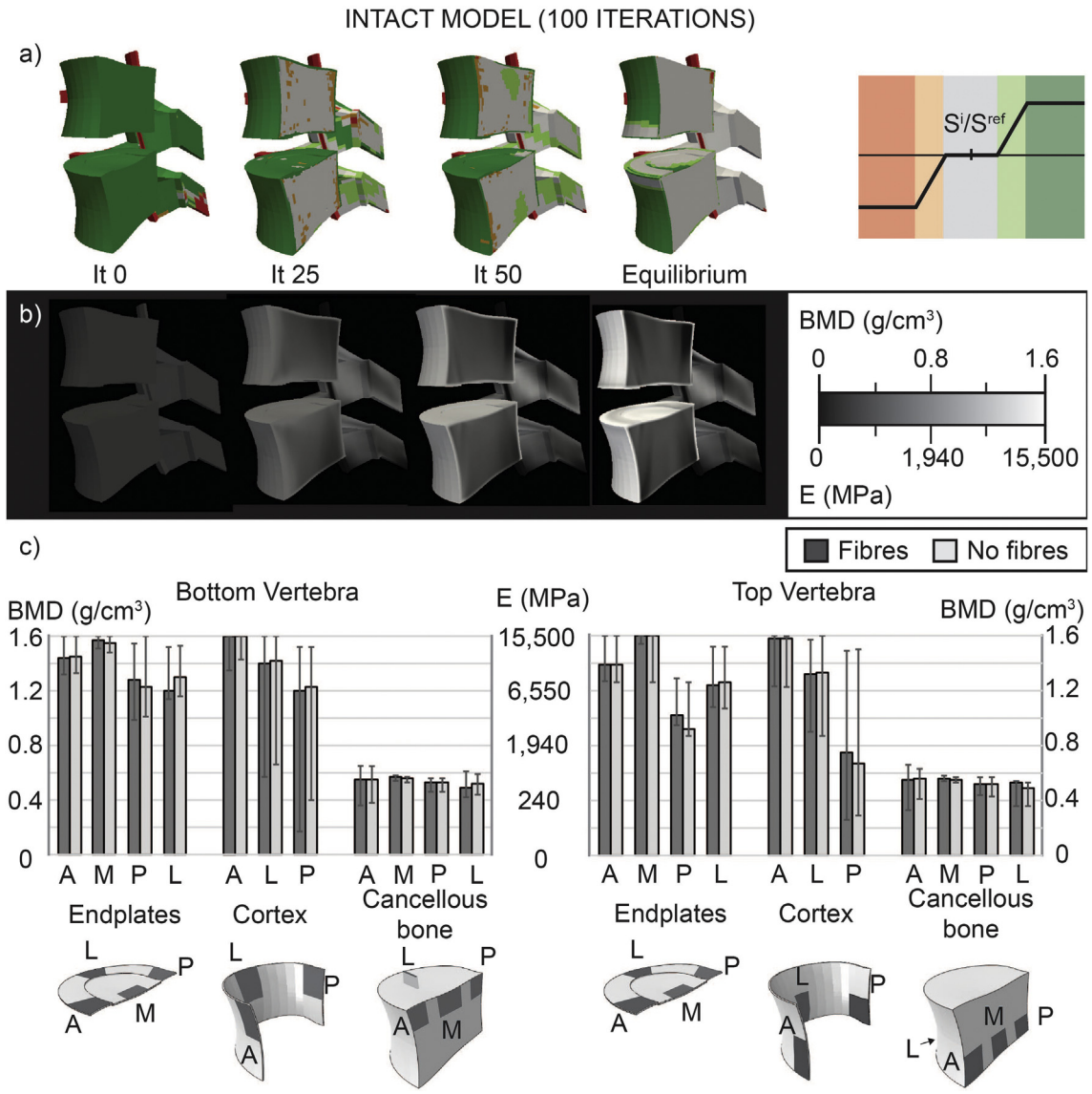

Fig. 2. Distribution of the mechanical stimulus (S/S_{ref}) (a) which drives the bone mineral density (BMD) and Young's modulus (E) change (b) during the bone-remodelling process of the intact segment with fibres. (c) BMD in different regions of the endplates, cortex and cancellous bone (P-posterior; M-middle; A-anterior; L-lateral) with and without fibres. Median and range values are shown.

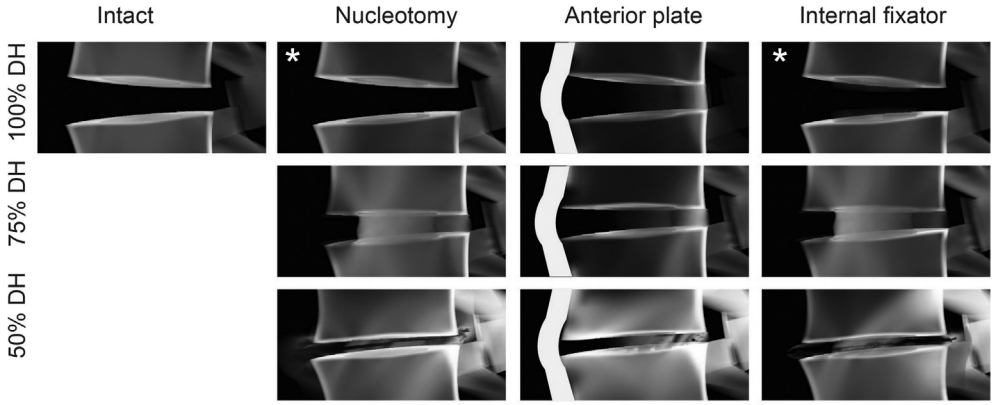

Fig. 3. X-ray-predicted images of the intact functional spinal unit and after equilibrium (no further changes in either vertebrae bone mineral density nor new tissue formation) for each treatment and disc height (DH) reduction. *Simulation failed because of excessive distortion resulting from the loss of stiffness. For the regions of new bone formations, the concentration of osteoblasts was used instead of BMD for a better visibility.

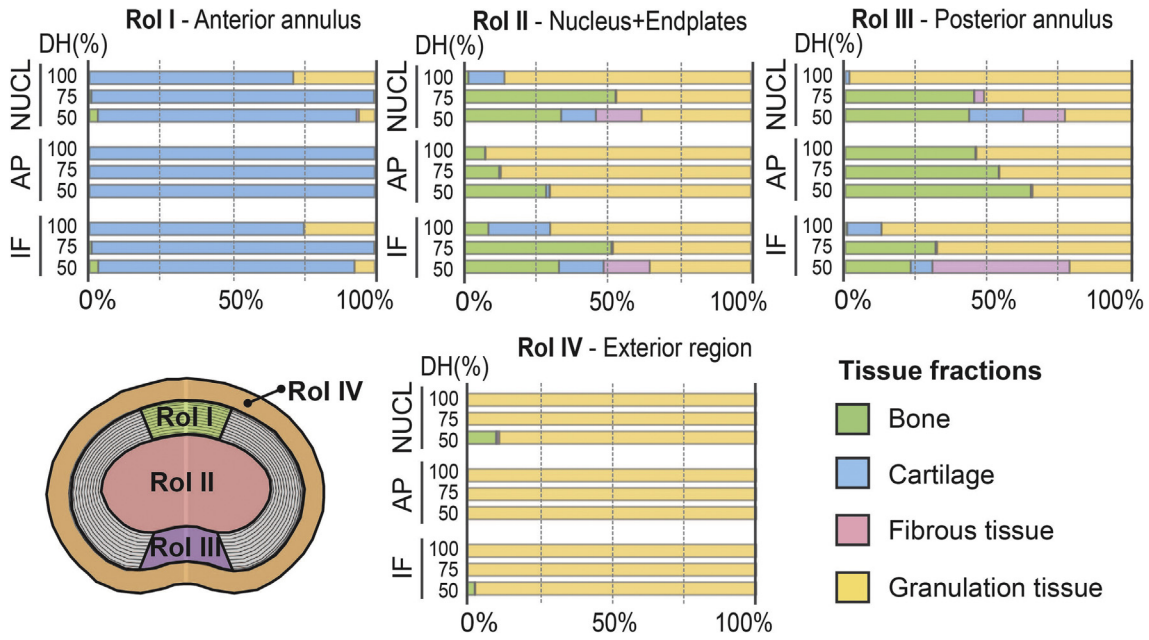

Fig. 4. Tissue distribution in each region of interest (RoI) after reaching equilibrium in each simulated scenario: nucleotomy (NUCL), anterior plate (AP) and internal fixator (IF) with different disc heights (DH). The posterior annulus corresponds to the annular defect. The values were calculated as the percentage of the total volume of each RoI. Bone existing in RoI IV indicates osteophyte formation.

anterior annulus elements. By contrast, an AP produced solid bone within the annular defect, which resulted in unloading of the facets and reduction of the BMD in the pedicles. With increasing DH loss, a gradual increase of the BMD in the pedicles was predicted, indicating higher facet loads. In turn, while an AP resulted in a higher bone density posteriorly, IF predicted a higher BMD anteriorly. A simple nucleotomy displayed little difference to IF. With 50% DH reduction, marked anterior and posterior osteophyte formations were predicted in both nucleotomy and IF, while a layer of cartilage and fibrous tissue remained in the mid-height disc region. The models with an AP did not display any signs of osteophytes.

The tissue composition at the end of each simulation was analysed in different regions of interests (RoI) (Fig. 4). These were defined to cover the anterior portion of the intact AF, the annular defect in the posterior region, the space left by the NP and EPs, and the area around the segment.

Considering the intact DH after nucleotomy, annular tissue destruction was predicted anteriorly because of high strains without instrumentation and with IF. By reducing the DH to 75%, bone fusion occurred in the posterior and central regions of the intervertebral space (RoIs II and III), with bone-volume fractions of 40–50%. On adding anterior instrumentation, the mechanical stimulus was greatly reduced, promoting intramembranous ossification in the posterior part of the annulus (RoI II).

Fig. 5 illustrates the healing process for the nucleotomy model with 75% DH. The mechanical stimulus (first row) determined the tissue phenotype that could potentially be formed in each element in each iteration; however, the progenitor-cell diffusion (second row) limited the tissue formation in the initial stage of the process. In turn, the vascularisation, which was kept constant throughout the simulation in the granular tissue and the outermost layer of the annulus (third row), and the bone neighbour condition (fourth row), which was activated when bony tissue filled 25% of the element volume, were necessary for bone formation. In this case, cartilage was formed in the space left by the resected tissue and was subsequently replaced by new bone through an endochondral ossification process, which started in the vertebral EPs and progressed towards the mid-height disc section until it fused the segment. No bone formation occurred in the remaining annulus because of the lack of vascularisation.

Immediately after nucleotomy, the mechanical environment of the segment changed, determining the progression of tissue healing (Fig. 6). Tissue destruction resulting from excessive strains led to a progressive increase in the flexibility for the nuclotomy and IF models with the intact DH (Fig. 6) and, consequently, to a failure of both models. However, the reduction in DH resulted in increased stiffness of the FSU, which developed further with tissue formation in all models. For nucleotomy, axial displacement initially increased to approximately 130% for 75% DH and gradually decreased to approximately 18% as the process progressed. Segmental rotation decreased initially to approximately 70% and further to approximately 13% of the intact value. Placing an IF for 75% DH, both axial displacement and segmental rotation decreased after the surgery and were reduced to 13 and 9%, respectively, once the tissue healed. For the models with 50% DH, the axial and rotational stiffness remained nearly constant throughout the simulation as a result of predicted non-union. By contrast, an AP resulted in stabilisation of the FSU under all DH conditions, with resulting axial displacement and segmental rotation <10% of the intact values for 100 and 75% DH and 3% for 50% DH.

3.3. Bone remodelling after surgery

The models predicted that the BMD adaptation within the vertebrae according to the altered mechanical environment would favour the force flow through the FSU (Fig. 3). In general, the BMD increased in the areas above and underneath the bone bridge and decreased in the regions where no bone formation was predicted. As such, application of the AP resulted in bone resorption anteriorly and increased the BMD posteriorly (Fig. 7a). The changes were not symmetrical about the disc mid-plane. The AP resulted in a decrease in the BMD in the posterior part of the upper EP, but in an increased BMD in the posterior part of the lower EP. For 50% DH, most of the models predicted a maximal BMD in all EP regions. Only the IF predicted a lower BMD in both EPs anteriorly for 50 and 75% DH. By contrast, the deformation of the EPs decreased in

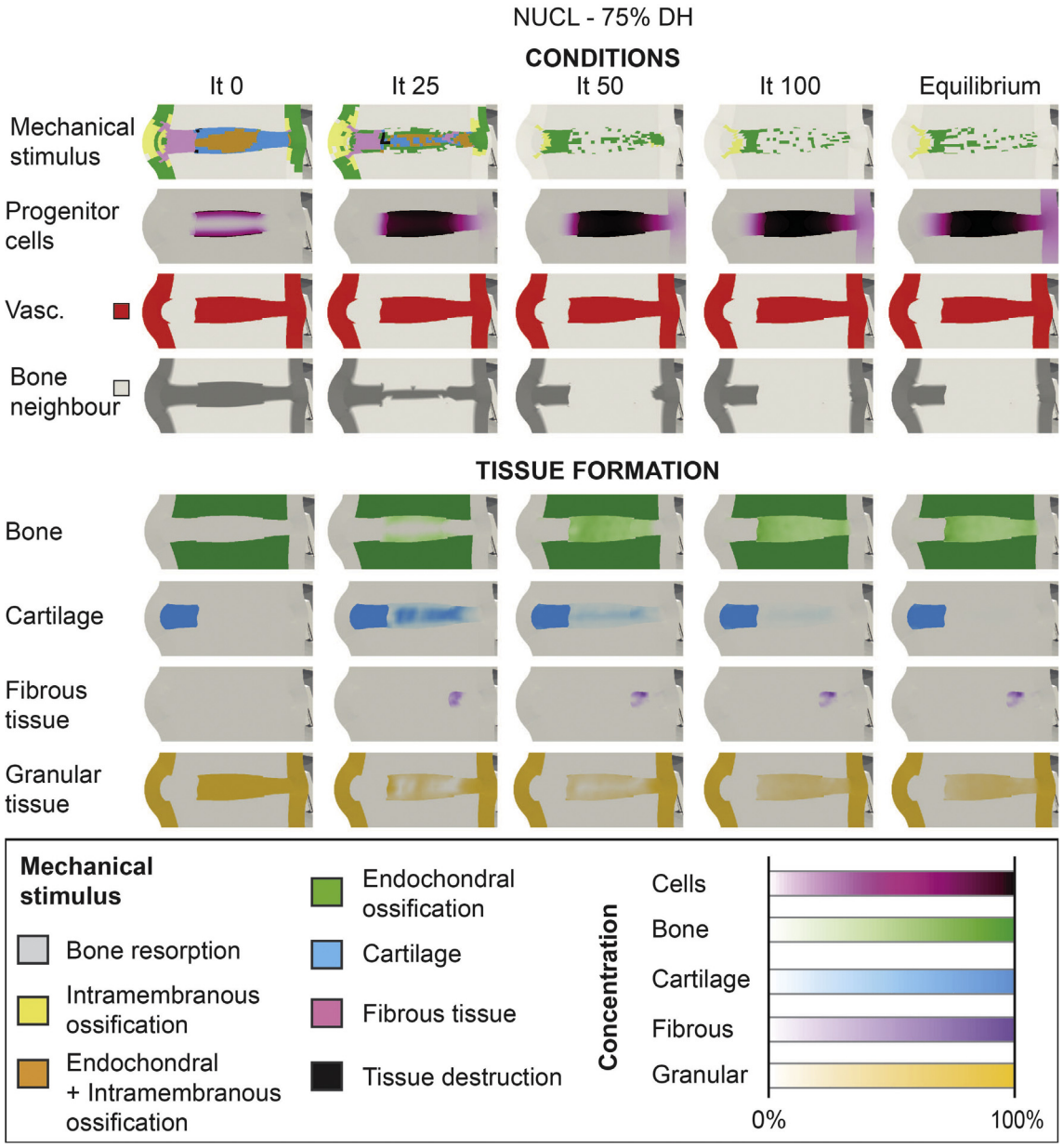

Fig. 5. Tissue-healing evolution in the model with nucleotomy (NUCL) and 75% disc height (DH). When all conditions for a tissue phenotype were met in an element, this tissue was formed proportional to the amount of precursor cells available.

the regions where the tissue was resected (NP and posterior AF) (Fig. 7b) but increased in the anterior portion of the AF immediately after nucleotomy. The adaptive response of the bony EPs tried to restore the intact deformation state. However, the formation of osteophytes provoked deflection of the cranial EP in the model with 50% DH, leading to denser EPs.

4. Discussion

In the present study, the mechanical conditions which may initiate the healing cascade from a mechanical point of view have been analysed together with the effect of each surgery on the vertebral bone density. An excessive range of motion has been shown to lead to tissue destruction and segment instability. Conversely, a lack of any strain prevented tissue formation. Bone-bridging promotion was shown to be possible by changing the mechanical scenario by adding instrumentation and/or decreasing the DH.

The adaptive bone-remodelling of the intact segment predicted denser bone in the anterior than in the posterior region of the vertebrae, in agreement with previous FE studies (Grosland and Goel, 2007) and medical-image observations (Antonacci et al., 1997; Silva et al., 1994). However, contrary to previous findings (Lowe et al., 2004), a higher BMD appeared at the central region of the EP than at the periphery as a result of the higher pressure transmitted through the NP.

By contrast, only a small influence of the annular fibres on the bone-density distribution was seen in the intact model, being even less after nucleotomy. Therefore, the hypothesis stated by Reitmaier et al. (2017), that bone bridging could be initiated by microtrauma in the AF could not be proven with the current model.

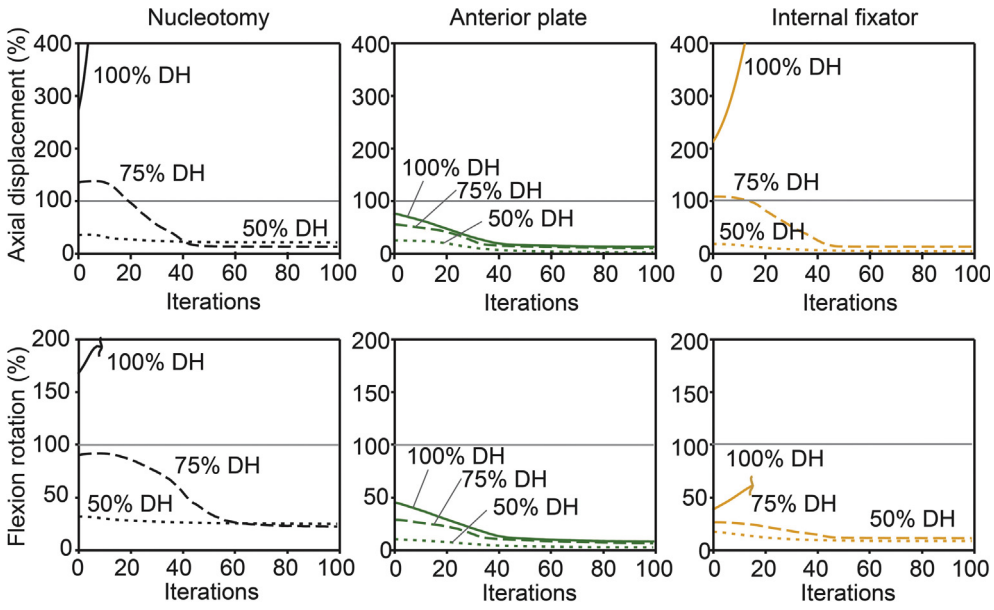

Fig. 6. Temporal evolution of axial displacement under compressive load and rotation under flexion moment with respect to the corresponding ranges of motion of the intact segment.

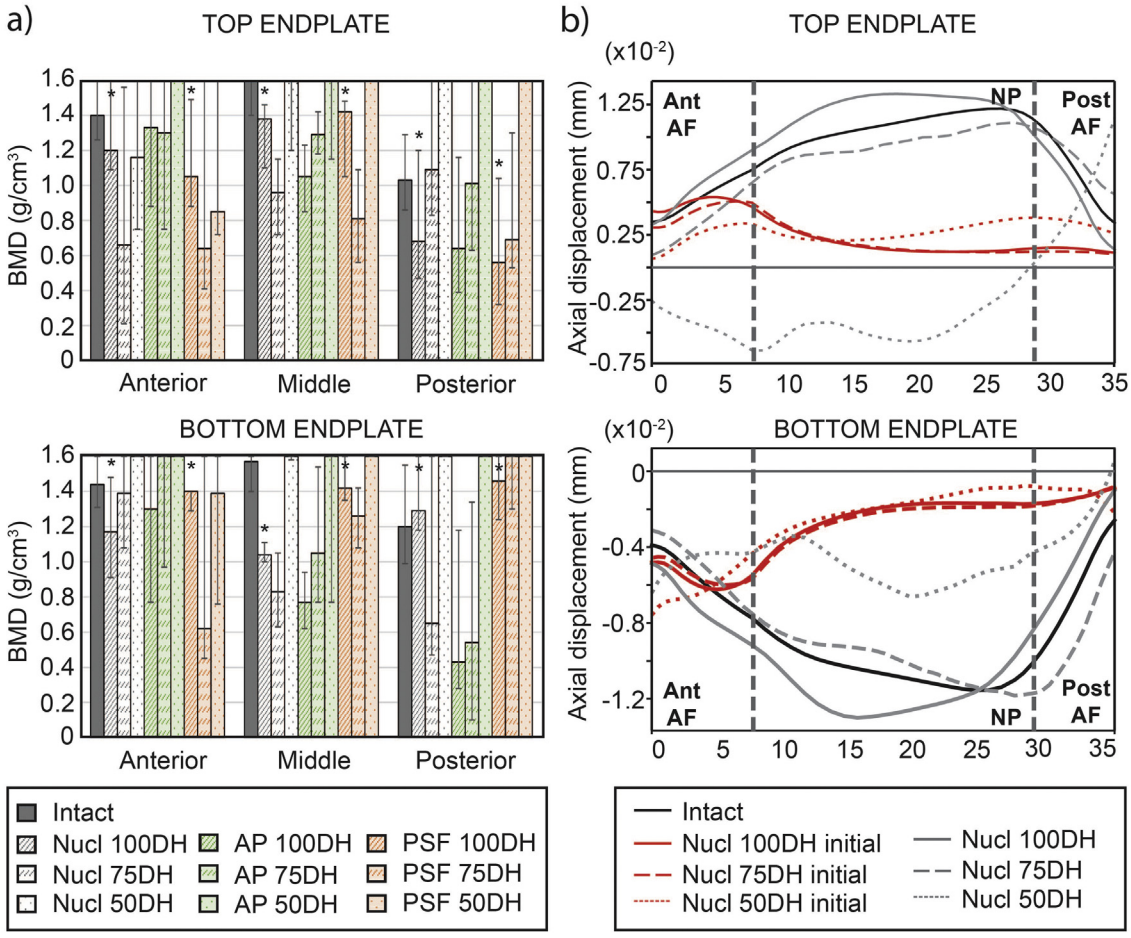

Fig. 7. (a) Bone mineral density (BMD) in different regions of the top and bottom endplates at the end of tissue healing for nucleotomy (Nucl), anterior plate (AP), and internal fixator (IF) models with different disc heights (DH). Median values and ranges are shown. *Simulation failed because of excessive distortion resulting from the loss of stiffness, thus the corresponding values are not representative. (b) Axial-displacement profiles in the mid-sagittal plane for the nucleotomy models immediately after the surgery and after the healing process, differentiating among anterior annulus fibrosus (Ant AF), nucleus pulposus (NP), and posterior annulus fibrosus (Post AF).

The inclusion of biological events, including possible fibrosis and ligament calcification, may help to shed light on this particular issue.

Progenitor-cell invasion resulting from the opening of the subchondral vascular network as a consequence of EP damage has been previously shown to be a possible trigger for bone bridging (Lowe et al., 2004; Tatsumi et al., 2015). Therefore, as was observed in animal studies, a nucleotomy with access to the vertebral vascular network might be as successful as instrumented fusion approaches (Crisco et al., 1990; Foster et al., 2002; Reitmaier et al., 2017; Toth et al., 2017). Not only animal studies have demonstrated the possibility of self-fusion, but some clinical studies have focused on the ability of the tissue to heal itself, producing similar outcomes with and without additional fixation (Jäger et al., 2003; Pourtaheri et al., 2015). In the present study, the cartilaginous EPs were entirely removed and the central region of the EP was exposed to the vascular network. Therefore, a source of cells was modelled at these sites. In accordance with the above-mentioned observations, segment fusion was predicted not only for instrumented cases but also for nucleotomy alone. Considering an intact DH, the segmental instability after nucleotomy or IF was too high, preventing tissue healing. A larger-diameter rod in the IF may help to reduce the RoM and promote bony fusion, but may also increase the risk of fixation loosening or breakage. Therefore, if the goal is to restore the DH, the use of an intervertebral spacer may be necessary. By contrast, AP placement was sufficiently stiff to promote posterior bony fusion. At the same time, one could clearly see the stress shielding effect of AP in the anterior region and in the vertebral bodies, where bone resorption was obvious. In case of 100% DH the high AP stiffness along with the bony fusion in the posterior part of the intervertebral space has led to a dramatic bone resorption within the posterior column. With 50% DH, the facet joint gap was already closed, which resulted in a more uniform load sharing between AP and the facet joints, however, stress shielding was still visible in the bone directly adjacent to AP. These results suggest that introduction of too stiff materials is not optimal and might induce a potentially dangerous situation of reduced bone quality.

The removal of disc tissue, together with possible tissue damage and further degeneration, was thought to cause a decrease in height. McGirt et al. (2009) found that large annular defects and less disc removal increased the risk of re-herniation, while a greater disc volume removal accelerated DH loss (up to 26% two years after surgery). Therefore, two different scenarios were simulated, decreasing the intact DH to 75 and 50%. A degree of controlled instability, as shown in the models with 75% DH, enhanced endochondral ossification, in agreement with ovine fusion models (Foster et al., 2002). However, a strong reduction of the DH may lead to ectopic bone formation, as was the case of the osteophytes formed with 50% DH, similar to the final stages of disc degeneration (Thompson et al., 1990).

4.1. Limitations and assumptions

In the present study, only a single motion segment was used. Therefore, this model does not allow investigating possible alterations in the adjacent segments, which is clinically a significant problem, also known as adjacent segment degeneration. Structural changes in the nucleotomised disc can result in altered load path in adjacent structures and thus induce adaptation processes, which in turn may affect the nucleotomised segment. Such investigations should be carried out in the future.

The tissue-healing algorithm employed was based on the theory of Claes & Heigele (1999) in defining linear elastic materials. Other healing theories proposed the inclusion of fluid flow (Prendergast et al., 1997) to calculate the mechanical stimulus, taking into account time-dependent effects in the tissue behaviour. However, because both theories have been shown to be able to predict spinal fusion (Postigo et al., 2014), the less extensive computationally was employed.

The vascularisation progress was not explicitly modelled and was maintained constant throughout the simulation, preventing bone formation in the remaining annular tissue. The degeneration of the tissue could cause tissue disruption and the entry of blood, allowing for additional bone formation in these regions. The sensitivity of the result due to changes in the threshold for bone-neighbour activation and the boundaries of the differentiation diagram should also be addressed in future studies. Finally, a continuous source of progenitor cells was considered at the EPs, which may cause an overestimation of the concentration of cells and tissue formation. Because the goal of this study was to determine possible explanations for the initiation of bone formation, all the above-mentioned assumptions were considered acceptable to cross-compare different mechanical scenarios. Validation using clinical data would be necessary for more reliable predictions.

The present study demonstrated that fusion may be self-induced by controlling the mechanical stabilisation without the need of additional fixation, thus reducing surgery costs and implant-related complications.

Conflict of interest

There is no conflict of interest.

Acknowledgments

This work was supported by the Spanish Ministry of Education, Culture and Sports, Spain (Grant FPU13/01070) and by the Spanish Ministry of Economy and Competitiveness, Spain (DPI2016-79302-R), as well as by the German Research Foundation, Germany (SCHM 2572/4-1, SCHM 2572/5-1).

References

Antonacci, M.D., Hanson, D.S., Leblanc, A., and Heggeness, M.H., 1997. Regional variation in vertebral bone density and trabecular architecture are influenced by osteoarthritic change and osteoporosis. Spine (Phila. Pa. 1976). 22, 2393–401; discussion 2401–2.

Argoubi, M., Shirazi-Adl, A., 1996. Poroelastic creep response analysis of a lumbar motion segment in compression. J. Biomech. 29, 1331–1339. https://doi.org/10.1016/0021-9290(96)00035-8.

Beaupré, G.S., Orr, T.E., Carter, D.R., 1990. An approach for time-dependent bone modeling and remodeling-application: a preliminary remodeling simulation. J. Orthop. Res. 8, 662–670. https://doi.org/10.1002/jor.1100080507.

Brinckmann, P., Frobin, W., Hierholzer, E., Horst, M., 1983. Deformation of the vertebral end-plate under axial loading of the spine. Spine (Phila. Pa. 1976) 8, 851–856.

Carter, D.R., 1984. Mechanical loading histories and cortical bone remodeling. Calcif. Tissue Int. 36 (Suppl 1), S19–S24.

Carter, D.R., Fyhrie, D.P., Whalen, R.T., 1987. Trabecular bone density and loading history: regulation of connective tissue biology by mechanical energy. J. Biomech. 20, 785–794.

Carter, D.R., Hayes, W.C., 1977. The compressive behavior of bone as a two-phase porous structure. J. Bone Joint Surg. Am. 59, 954–962.

Chazal, J., Tanguy, A., Bourges, M., et al., 1985. Biomechanical properties of spinal ligaments and a histological study of the supraspinal ligament in traction. J. Biomech. 18, 167–176. https://doi.org/10.1016/0021-9290(85)90202-7.

Claes, L.E., Heigele, C.A., 1999. Magnitudes of local stress and strain along bony surfaces predict the course and type of fracture healing. J. Biomech. 32, 255–266.

Crisco, J.J., Panjabi, M.M., Wang, E., et al., 1990. The injured canine cervical spine after six months of healing. An in vitro three-dimensional study. Spine (Phila. Pa. 1976) 15, 1047–1052.

Foster, M.R., Allen, M.J., Schoonmaker, J.E., et al., 2002. Characterization of a developing lumbar arthrodesis in a sheep model with quantitative instability. Spine J. 2, 244–250. https://doi.org/10.1016/S1529-9430(02)00189-4.

Frei, H., Oxland, T.R., Rathonyi, G.C., Nolte, L.P., 2001. The effect of nucleotomy on lumbar spine mechanics in compression and shear loading. Spine (Phila. Pa. 1976) 26, 2080–2089. https://doi.org/10.1097/00007632-200110010-00007.

Goel, V.K., Monroe, B.T., Gilbertson, L.G., Brinckmann, P., 1995. Interlaminar shear stresses and laminae separation in a disc. Finite element analysis of the L3–L4

motion segment subjected to axial compressive loads. Spine (Phila. Pa. 1976) 20, 689–698.
Grosland, N.M., Goel, V.K., 2007. Vertebral endplate morphology follows bone remodeling principles. Spine (Phila. Pa. 1976) 32, E667–E673. https://doi.org/10.1097/BRS.0b013e318158cfaf.
Holm, S., 1993. Pathophysiology of disc degeneration. Acta Orthop. Scand. Supplement, 13–15.
Holzapfel, G.a., Schulze-Bauer, C.a.J., Feigl, G., Regitnig, P., 2005. Single lamellar mechanics of the human lumbar anulus fibrosus. Biomech. Model. Mechanobiol. 3, 125–140. https://doi.org/10.1007/s10237-004-0053-8.
Huiskes, R., Weinans, H., Grootenboer, H.J., et al., 1987. Adaptive bone-remodeling theory applied to prosthetic-design analysis. J. Biomech. 20, 1135–1150. https://doi.org/10.1016/0021-9290(87)90030-3.
Isaksson, H., van Donkelaar, C.C., Huiskes, R., Ito, K., 2008. A mechano-regulatory bone-healing model incorporating cell-phenotype specific activity. J. Theor. Biol. 252, 230–246. https://doi.org/10.1016/j.jtbi.2008.01.030.
Ivicsics, M.F., Bishop, N.E., Püschel, K., et al., 2014. Increase in facet joint loading after nucleotomy in the human lumbar spine. J. Biomech. 47, 1712–1717. https://doi.org/10.1016/j.jbiomech.2014.02.021.
Jäger, M., Seller, K., Raab, P., et al., 2003. Clinical outcome in monosegmental fusion of degenerative lumbar instabilities: instrumented versus non-instrumented. Med. Sci. Monit. 9, CR324-R327.
Kelly, D.J., Prendergast, P.J., 2005. Mechano-regulation of stem cell differentiation and tissue regeneration in osteochondral defects. J. Biomech. 38, 1413–1422. https://doi.org/10.1016/j.jbiomech.2004.06.026.
Lacroix, D., Prendergast, P.J., 2002. A mechano-regulation model for tissue differentiation during fracture healing: analysis of gap size and loading. J. Biomech. 35, 1163–1171.
Lowe, T.G., Hashim, S., Wilson, L.a., et al., 2004. A biomechanical study of regional endplate strength and cage morphology as it relates to structural interbody support. Spine (Phila. Pa. 1976) 29, 2389–2394. https://doi.org/10.1097/01.brs.0000143623.18098.e5.
Lu, Y.M., Hutton, W.C., Gharpuray, V.M., 1996. Can variations in intervertebral disc height affect the mechanical function of the disc? Spine (Phila. Pa. 1976) 21, 2208–2216. https://doi.org/10.1097/00007632-199610010-00007.
Maroon, J.C., 2002. Current concepts in minimally invasive discectomy. Neurosurgery 51, 137–145. https://doi.org/10.1227/01.NEU.0000031066.08137.64.
McGirt, M.J., Eustacchio, S., Varga, P., et al., 2009. A Prospective cohort study of close interval computed tomography and magnetic resonance imaging after primary lumbar discectomy. Spine (Phila. Pa. 1976) 34, 2044–2051. https://doi.org/10.1097/BRS.0b013e3181b34a9a.
Mullender, M.G., Huiskes, R., 1995. Proposal for the regulatory mechanism of Wolff's law. J. Orthop. Res. 13, 503–512. https://doi.org/10.1002/jor.1100130405.
Nakamura, T., Okada, T., Endo, M., et al., 2014. Angiopoietin-like protein 2 induced by mechanical stress accelerates degeneration and hypertrophy of the ligamentum flavum in lumbar spinal canal stenosis. PLoS One 9, e85542.
Nasser, R., Yadla, S., Maltenfort, M.G., et al., 2010. Complications in spine surgery. J. Neurosurg. Spine 13, 144–157. https://doi.org/10.3171/2010.3.SPINE09369.
Panjabi, M.M., Goel, V., Oxland, T., 1992. Human lumbar vertebrae: quantitative three-dimensional anatomy. Spine (Phila. Pa. 1976) 17, 299–306.
Panjabi, M.M., Oxland, T., Takata, K., et al., 1993. Articular facets of the human spine. Quantitative three-dimensional anatomy. Spine (Phila. Pa. 1976). 18, 1298–1310. https://doi.org/10.1097/00007632-199308000-00009.
Pateder, D.B., Benzel, E., 2010. Noninstrumented facet fusion in patients undergoing lumbar laminectomy for degenerative spondylolisthesis. J. Surg. Orthop. Adv. 19, 153–158.
Pintar, F.A., Yoganandan, N., Myers, T., et al., 1992. Biomechanical properties of human lumbar spine ligaments. J. Biomech. 25, 1351–1356.
Postacchini, F., Postacchini, R., 2011. Operative management of lumbar disc herniation: the evolution of knowledge and surgical techniques in the last century. Acta Neurochir. Suppl. 108, 17–21. https://doi.org/10.1007/978-3-211-99370-5_4.
Postigo, S., Schmidt, H., Rohlmann, A., et al., 2014. Investigation of different cage designs and mechano-regulation algorithms in the lumbar interbody fusion process – a finite element analysis. J. Biomech. 47, 1514–1519. https://doi.org/10.1016/j.jbiomech.2014.02.005.
Pourtaheri, S., Billings, C., Bogatch, M., et al., 2015. Outcomes of instrumented and noninstrumented posterolateral lumbar fusion. Orthopedics 38, e1104–e1109. https://doi.org/10.3928/01477447-20151120-07.
Prendergast, P.J., Huiskes, R., Søballe, K., 1997. Biophysical stimuli on cells during tissue differentiation at implant interfaces. J. Biomech. 30, 539–548. https://doi.org/10.1016/S0021-9290(96)00140-6.
Putzier, M., Schneider, S.V., Funk, J.F., et al., 2005. The surgical treatment of the lumbar disc prolapse: nucleotomy with additional transpedicular dynamic stabilization versus nucleotomy alone. Spine (Phila. Pa. 1976) 30, E109–E114.
Reitmaier, S., Schuelke, J., Schmidt, H., et al., 2017. Spinal fusion without instrumentation – experimental animal study. Clin. Biomech. 46, 6–14. https://doi.org/10.1016/j.clinbiomech.2017.04.008.
Rohlmann, A., Consmüller, T., Dreischarf, M., et al., 2014. Measurement of the number of lumbar spinal movements in the sagittal plane in a 24-hour period. Eur. Spine J. 23, 2375–2384. https://doi.org/10.1007/s00586-014-3588-0.
Schmidt, H., Galbusera, F., Rohlmann, A., et al., 2012. Effect of multilevel lumbar disc arthroplasty on spine kinematics and facet joint loads in flexion and extension: a finite element analysis. Eur. Spine J. 21, 663–674. https://doi.org/10.1007/s00586-010-1382-1.
Schmidt, H., Heuer, F., Drumm, J., et al., 2007. Application of a calibration method provides more realistic results for a finite element model of a lumbar spinal segment. Clin. Biomech. 22, 377–384. https://doi.org/10.1016/j.clinbiomech.2006.11.008.
Schmidt, H., Heuer, F., Simon, U., et al., 2006. Application of a new calibration method for a three-dimensional finite element model of a human lumbar annulus fibrosus. Clin. Biomech. 21, 337–344. https://doi.org/10.1016/j.clinbiomech.2005.12.001.
Shefelbine, S.J., Augat, P., Claes, L., Simon, U., 2005. Trabecular bone fracture healing simulation with finite element analysis and fuzzy logic. J. Biomech. 38, 2440–2450. https://doi.org/10.1016/j.jbiomech.2004.10.019.
Shirazi-Adl, A., Ahmed, A.M., Shrivastava, S.C., 1986. Mechanical response of a lumbar motion segment in axial torque alone and combined with compression. Spine (Phila. Pa. 1976) 11, 914–927.
Silva, M.J., Wang, C., Keaveny, T.M., Hayes, W.C., 1994. Direct and computed tomography thickness measurements of the human, lumbar vertebral shell and endplate. Bone 15, 409–414. https://doi.org/10.1016/8756-3282(94)90817-6.
Smit, T.H., 1996. The mechanical significance of the trabecular bone architecture in a human vertebra. Book, 1–127.
Tatsumi, R., Lee, Y.-P., Khajavi, K., et al., 2015. In vitro comparison of endplate preparation between four mini-open interbody fusion approaches. Eur. Spine J. https://doi.org/10.1007/s00586-014-3708-x.
Thompson, J.P., Pearce, R.H., Schechter, M.T., et al., 1990. Preliminary evaluation of a scheme for grading the gross morphology of the human intervertebral disc. Spine (Phila. Pa. 1976) 15, 411–415.
Toth, J.M., Foley, K.T., Wang, M., et al., 2017. Is lumbar facet fusion biomechanically equivalent to lumbar posterolateral onlay fusion? J. Neurosurg. Spine 26, 586–593. https://doi.org/10.3171/2016.10.SPINE16649.
Uhthoff, H.K., Rahn, B.A., 1981. Healing patterns of metaphyseal fractures. Clin. Orthop. Relat. Res., 295–303
Urban, J.P.G., 1993. The effect of physical factors on disc cell metabolism. In: Buckwalter, J.A., Goldberg, V.M., Woo, S.-Y. (Eds.), Musculoskeletal Soft Tissue Aging: Impact on Mobility. American Academy of Orthopaedic Surgeons, Rosemont, IL, pp. 391–412.
Wang, J.Z., Fang, X.T., Lv, E., et al., 2015. TGF-beta1 related inflammation in the posterior longitudinal ligament of cervical spondylotic myelopathy patients. Int. J. Clin. Exp. Med. 8, 2233–2239.
Wood, R.A., Favor, R.J., 1972. Titanium Alloys Handbook. Center, Airforce Materials Laboratory. Metals, Ceramics Information.